CONF-860421--40

INFLUENCE OF TEMPERATURE AND LITHIUM PURITY ON CORROSION OF FERROUS ALLOYS IN A FLOWING LITHIUM ENVIRONMENT*

O. K. Chopra and D. L. Smith

Materials Science and Technology Division
Argonne National Laboratory
Argonne, Illinois 60439

CONF-860421--40

DE86 010507

March 1986

For presentation at the Second International Conference on Fusion Reactor Materials, Chicago, IL, April 13-17, 1986, and publication in the Journal of Nuclear Materials.

*Work supported by the Office of Fusion Energy, U. S. Department of Energy, under Contract W-31-109-Eng-38.

EAB

INFLUENCE OF TEMPERATURE AND LITHIUM PURITY ON CORROSION OF FERROUS ALLOYS IN A FLOWING LITHIUM ENVIRONMENT

O. K. Chopra and D. L. Smith

Materials Science and Technology Division
Argonne National Laboratory
Argonne, IL 60439, U.S.A.

Abstract

Corrosion data have been obtained on ferritic HT-9 and Fe-9Cr-1Mo steel and austenitic Type 316 stainless steel in a flowing lithium environment at temperatures between 372 and 538°C. The corrosion behavior is evaluated by measurements of weight loss as a function of time and temperature. A metallographic characterization of materials exposed to a flowing lithium environment is presented.

INFLUENCE OF TEMPERATURE AND LITHIUM PURITY ON CORROSION OF FERROUS ALLOYS IN A FLOWING LITHIUM ENVIRONMENT

O. K. Chopra and D. L. Smith

Materials Science and Technology Division
Argonne National Laboratory
Argonne, IL 60439, U.S.A.

1. Introduction

Liquid lithium is an attractive first wall/blanket material for fusion reactors because of its efficient heat transfer properties and acceptable tritium-breeding characteristics. A major concern arising from the use of lithium is its compatibility with the containment material. The corrosion behavior of several ferritic and austenitic steels has been investigated in thermal- and forced-circulation lithium loops [1-10]. Data on corrosion/mass transfer in liquid lithium systems have been reviewed to identify the influence of various material and system parameters on corrosion [11-13]. The results indicate that mass transfer and deposition most likely will determine the maximum operating temperature in liquid lithium blanket systems. The ferritic HT-9 alloy and Fe-9Cr-1Mo steel exhibit better resistance to corrosion in lithium than the austenitic steels, such as Type 316 stainless steel (SS). However, available data are insufficient to quantify the influence of system parameters, e.g., temperature, flow velocity, system temperature gradient (ΔT), lithium purity, etc., on corrosion and to estimate the maximum operating temperature limits for liquid lithium systems. This paper presents information on the corrosion behavior of several ferrous alloys in a flowing lithium environment at temperatures between 372 and 538°C. The effects of temperature and lithium purity on corrosion are discussed.

2. Experimental Procedure

The corrosion tests were conducted in a forced-circulation lithium loop consisting of three test vessels and a secondary cold-trap purification loop. A detailed description of the lithium loop has been presented earlier [1]. Flat corrosion specimens, ~70 x 10 x 0.3 mm in size, of ferritic HT-9 and Fe-9Cr-1Mo steels and austenitic Type 316 SS were exposed to flowing lithium, and the corrosion behavior was evaluated from measurements of weight loss and the depth of internal corrosion (or thickness of the ferrite layer for austenitic steels). The chemical composition of the materials is given in table 1. The ferritic steels were exposed in the normalized and tempered condition while Type 316 SS was in the solution annealed or 20% cold-worked (CW) condition.

Specimens were periodically removed from the loop and cleaned in alcohol and water, and the weight-loss data were obtained at different exposure times. Tests were conducted in the test vessel as well as in the specimen exposure vessel. The lithium flow was from the test vessel to the specimen exposure vessel. The temperature and time of exposure and the loop operating conditions for the various test runs are given in table 2. Lithium was recirculated at ~1 ℓ/min in the primary loop, and the concentrations of C and H in lithium were ~10 and 120 wppm, respectively. The nitrogen content is given in table 2.

3. Results

3.1. Ferritic steels

The weight losses for HT-9 and Fe-9Cr-1Mo steels exposed to flowing lithium at 372, 427, 482, and 538°C are shown in fig. 1. The results indicate that after a relatively large weight loss durig the initial 500-h exposure to lithium, the weight losses for ferritic steels follow a linear law with time

and yield a constant dissolution rate. At all temperatures, the weight losses and dissolution rates for the HT-9 alloy and Fe-9Cr-1Mo steel are comparable. Furthermore, the specimens exposed at 427°C during test runs 4 and 5 show identical dissolution behavior although the location of these specimens was different, i.e., specimens were placed in the test vessel at the maximum loop temperature in run 5 while the specimens in run 4 were located downstream in the specimen exposure vessel. The dissolution rates for both ferritic steels decrease with a decrease in temperature.

The ferritic steel specimens exposed during run 6 at 482°C in the specimen exposure vessel, i.e., a location downstream from the specimens exposed at 538°C, showed very small weight loss. Eight separate specimens exposed for 1500 to 2500 h at 482°C showed weight losses of between 0.2 and 0.4 g/m^2. For these specimens, most of the weight loss occurred during the initial 500 h and the specimens showed little or no weight loss for longer exposures. Such effects of specimen location, or downstream effects, were not observed for other test runs. Downstream effects have been observed in flowing lithium at 538°C [7], e.g., the dissolution rates of Fe-9Cr-1Mo or Fe-2 1/4Cr-1Mo decreased by ~30% over a distance of 152 mm in the isothermal test section.

The corrosion specimens were examined metallographically to characterize the compositional and microstructural changes. Micrographs of the surface of HT-9 specimens exposed to lithium for ~5000 h at 372, 427, and 482°C are shown in fig. 2. All specimens exhibit a pebbled or dimpled appearance. Such dimples are fully developed after the initial ~1500-h exposure and their size does not change with additional exposure. The large weight losses observed during the initial stages of exposure may be attributed to the formation of the dimpled surface appearance. Micrographs of the surface of HT-9 specimens

exposed to lithium at 538 and 482°C during run 6 are shown in fig. 3. The specimen exposed at 538°C developed a dimpled appearance. Figures 2 and 3 indicate that the size of the dimples increases with an increase in temperature, i.e., the size increases from 0.5-2 μm at 372°C to 2-6 μm at 538°C. Specimens that were exposed downstream at 482°C during run 6 show surface deposits and the dimpled structure is not fully developed. X-ray analyses indicate that the surface deposits are primarily iron. The presence of deposits and the absence of a sharp dimpled structure may account for the relatively small weight losses observed for these specimens.

Energy dispersive x-ray analyses (EDAX) were performed to determine the differences in surface composition of HT-9 alloy exposed to lithium at different temperatures. The weight loss and concentrations of major elements for the corrosion specimens are given in table 3. The results indicate that the formation of a dimpled structure and the initial weight loss are associated with depletion of chromium from the steel to achieve an equilibrium surface composition, which appears to depend on system parameters, e.g., temperature, lithium purity, location, etc. The concentration of chromium in the alloy surface decreases from ~12% to between 6 and 8%; the values after exposure at 538°C are lower than those at 372°C. The equilibrium value of surface composition is achieved after ~1500 h of exposure at the higher temperatures, e.g., 482°C. Specimens that do not develop a sharp dimpled structure, e.g., specimens exposed for <1500 h or the specimens exposed downstream at 482°C during run 6, show little or no depletion of chromium and small initial weight loss. It will be shown in the next sections that the initial weight loss and the surface composition and morphology are related to chemical reactions between alloy elements and nitrogen in lithium.

3.2. Austenitic steels

The corrosion behavior of annealed and 20% CW Type 316 SS in flowing lithium at 372, 427, 482, and 538°C is shown in figs. 4 and 5. The weight losses for the austenitic steels are more than an order of magnitude greater than those for the ferritic steels. The significant results are summarized as follows:

(a) The weight-loss data increase linearly with time and achieve a steady-state dissolution rate after an initial ~1500-h transient period characterized by a large loss in weight. The weight losses for 20% CW steel are comparable to or slightly higher than those for the annealed steel.

(b) The initial weight losses for the various corrosion test specimens show significant scatter. Differences in weight-loss data are often observed for specimens exposed separately at different times but at the same temperature (fig. 5). However, duplicate specimens exposed at the same time always exhibit identical dissolution behavior (fig. 4).

(c) The weight losses after the transient stage do not exhibit a correlation with test temperature. Specimens exposed at the maximum loop temperature of 427 or 482°C lose 15 to 30 g/m^2 while the specimens exposed at 538°C lose <15 g/m^2. Three of the four specimens of annealed Type 316 SS exposed at 538°C lost ~3 g/m^2 after 500 h (fig. 5a). Specimens exposed at 372°C also show insignificant loss in weight during the transient stage.

(d) Irrespective of the initial weight loss, the steady-state dissolution rates of annealed or 20% CW Type 316 SS are

independent of temperature, i.e., the rates are approximately the same at all test temperatures. However, the dissolution rates for a set of specimens exposed at 427°C during run 5 (shown by triangles in fig. 4) are a factor of 3 to 4 higher than those for the other specimens.

(e) The initial weight losses at 427 and 482°C are comparable to those predicted from the steady-state dissolution rates over a period of two years.

After exposure to lithium, the austenitic stainless steel specimens develop a porous ferrite layer that is depleted significantly in nickel and contains a 5 to 10 μm surface region depleted also in chromium. The concentration of nickel decreases rapidly across the ferrite-austenite phase boundary. Measurements of the thickness of the ferrite layer indicate that a "stoichiometric" steady-state dissolution behavior (i.e., when the elements being dissolved are in proportion to their concentration in the steel) is not achieved in a flowing lithium environment [1]. The thickness of the ferrite layer increases with time.

Metallographic examination of the austenitic steel specimens indicates that the weight-loss data are related to the composition and morphology of the ferrite layers. Typical surface morphologies for the austenitic steel specimens are shown in figs. 6 and 7. Specimens that show large weight losses develop a sharp dimpled surface with large cavities or porosity (e.g., at 427 and 482°C, fig. 6) while the specimens with small weight losses develop a poorly defined dimpled structure (e.g., at 372°C, fig. 6) or a cellular structure (fig. 7). At 538°C, the specimen with the largest weight loss (shown as diamond symbols in fig. 5) develop a dimpled structure and the other specimens, with smaller weight losses (square and triangle symbols), exhibit a

cellular structure. The cellular surface appearance is generally observed during the early stages of the transient period and is typical of austenitic stainless steels exposed for >2000 h at temperatures above 400°C.

The ferrite layers formed on 20% CW Type 316 SS exposed during runs 4 and 5 for >5000 h at 427°C are shown in fig. 8. The ferrite layers are significantly different for the two specimens exposed under similar time and temperature conditions. The specimen exposed during run 4 has uniform porosity, while the specimen from run 5 has a layered structure, viz., the outer 15-μm-thick region has very large cavities. The high dissolution rates observed for these specimens from run 5 may be attributed to the large cavities in the ferrite layer.

The weight loss and concentrations of major elements for annealed Type 316 SS exposed to flowing lithium at different temperatures are given in table 4. Similar results were obtained for 20% CW Type 316 SS. The results indicate that the depletion of nickel from the steel is quite rapid. The concentration of nickel decreases from 12.9 to <1% for the specimens that exhibit a sharp dimpled structure and surface porosity. The nickel content is slightly higher, i.e., 1.5 to 2.5%, after exposure at 372°C and for the specimens that develop a cellular structure at 538°C. The depletion of chromium from the steel is slower and related to chemical reactions between alloy elements and nitrogen in lithium. Such reactions appear to depend on system parameters such as lithium purity, loop ΔT, location (downstream effects), etc. The concentration of chromium decreases from ~18% to between 8 and 10%. Limited data indicate that specimens exposed at 482°C in lithium containing ~250 wppm nitrogen (i.e., run 2) show greater depletion of chromium and weight loss than those exposed for similar times in lithium with <100 wppm nitrogen.

Corrosion specimens that were exposed downstream in the specimen exposure vessel often contain surface deposits. For most specimens, the deposits were in the form of stringers, while the deposits on some specimens had a distinct crystallographic orientation relative to the base metal. The EDAX data indicate that these specimens contain chromium-rich deposits; the surface chromium content is >20%.

3.3. Dissolution rates

The steady-state dissolution rates of the various sets of ferritic steels and Type 316 SS exposed to flowing lithium are given in table 5. The Arrhenius plots of the data are shown in fig. 9. The results indicate that the dissolution rates for HT-9 and Fe-9Cr-1Mo steel increase by a factor of ~10 when the temperature increases from 400 to 550°C. The Arrhenius plot for the dissolution rates yields an activation energy of 16.3 kcal/mole. However, the dissolution rates for Type 316 SS are insensitive to changes in temperature. The steady-state dissolution rates range between 1.5 and 2.5 $mg/m^2 \cdot h$; the values are higher at lower temperatures.

For the ferritic steels, the temperature dependence of dissolution rates in lithium (i.e., activation energy Q = 16.3 kcal/mole) is lower than that observed in flowing Pb-17Li (i.e., Q = 22.1 kcale/mole) [14] and comparable to that observed in flowing sodium (i.e., Q = 17.5 kcal/mole) [15]. In flowing sodium, the dissolution rates of ferritic steels are very sensitive to the oxygen content in sodium. Limited data in flowing lithium indicate that an increase in nitrogen in lithium increases the dissolution rates. For example, the weight loss for HT-9 at 482°C in lithium containing ~250 wppm nitrogen, run 2 (table 3), is a factor of ~3 greater than it is in lithium with ~100 wppm nitrogen. The data in fig. 10 were obtained in lithium containing

≤100 wppm nitrogen. The influence of nitrogen on the dissolution behavior of ferritic steels needs to be established quantitatively.

The dissolution rates of austenitic Type 316 SS show an anomalous behavior, i.e., the rates are insensitive to a change in temperature and are the same at temperatures between 372 and 538°C. However, the data for total weight loss show significant variation. The large weight losses for austenitic steels arise primarily from the depletion of nickel from the steel and the alloy surfaces develop a porous ferrite scale. For most specimens, the surface nickel content is <1% irrespective of the temperature of exposure or total weight loss of the specimens. However, the depletion of chromium is greater for specimens that show large weight loss and porosity, e.g., specimens exposed in high-nitrogen lithium (run 2). Nitrogen can react with alloy elements and lithium to form stable ternary nitrides, such as Li_9CrN_5 and Li_3FeN_2, and thus accelerate the dissolution process of ferrous alloys [16]. These results indicate that dissolution of alloy elements as well as chemical reactions between interstitial elements and alloys influence the overall corrosion behavior of structural materials in lithium. The formation of reaction products, e.g., ternary nitrides, on the alloy surfaces may influence the dissolution of alloy elements (particularly nickel) from austenitic steels.

The ternary nitrides are soluble in alcohol or water and, therefore, are not observed on clean corrosion specimens. The presence of the ternary nitrides was investigated by chemical analysis of the alcohol used for cleaning HT-9 or Type 316 SS specimens exposed for ~500 h in lithium at 538°C and 482°C (downstream location). The solutions were filtered before the analysis. The concentrations of major elements expressed as wppm of lithium dissolved in the methanol solutions are given in table 6. The solutions used

for cleaning the corrosion specimens contain significant amounts of Cr, Fe, and Mo. The Ni content in these solutions is the same as that in lithium solutions. The residues collected from the solutions contained primarily Cr and Fe. Ultraviolet-visible absorption spectroscopy of the solutions show that the chromium is present in the 6^+ oxidation state. These results indicate that corrosion products are present on the alloy surfaces and that these products are ternary nitrides of Cr and Fe.

4. Conclusions

Corrosion data for ferritic HT-9 and Fe-9Cr-1Mo steel in flowing lithium at temperatures between 372 and 538°C indicate that after an initial transient period of ~500 h, the weight losses for ferritic steels increase linearly with time and yield a constant dissolution rate. The dissolution rates increase with a increase in temperature. An Arrhenius plot of the dissolution rates yields an activation energy of 16.3 kcal/mole. The dissolution behavior of the two steels is identical. After exposure to lithium, the alloy surfaces develop a dimpled appearance. A dimpled surface structure is fully developed after ~2000 h of exposure and the size of the dimples does not change with additional exposure. However, the size of dimples decreases with a decrease in temperature. The formation of a dimpled structure is associated with depletion of chromium from the alloy surface and leads to significant weight loss during the initial period of exposure. Limited data (i.e., Run 6) indicate some downstream effects on the dissolution behavior of alloys. Iron-rich deposits were observed on the surfaces of HT-9 and Fe-9Cr-1Mo specimens located downstream (at 482°C) from the maximum loop temperature position (538°C). These specimens showed little or no weight loss.

The dissolution rates for austenitic Type 316 SS reach a steady state after an initial ~1500-h period characterized by rapid dissolution. The

steady-state dissolution rates are relatively insensitive to variations in temperature. The dissolution rates for annealed or 20% CW Type 316 stainless steel exposed to lithium at temperatures between 372 and 538°C range from 1.5 to 2.5 $mg/m^2 \cdot h$. The weight losses after the initial transient stage (i.e., 500- to 1000-h exposure) range between 15 and 30 g/m^2 after exposure at 427 or 482°C and between 3 and 15 g/m^2 after exposure at 372 or 538°C. The initial dissolution stage is associated with the formation of a ferritic surface layer due to depletion of nickel and, to some extent, chromium from the steel. This transient stage appears to play an important role in controlling the nature of the surface modifications and, consequently, in the overall dissolution behavior of austenitic steels. Specimens with large weight losses develop a well-defined dimpled structure and deep cavities. The surfaces of these specimens are depleted of nickel, and the chromium content ranges from 8 to 10%. Specimens with small weight losses, i.e., <10 g/m^2, develop a very fine dimpled structure (e.g., at 372°C) or a cellular structure (e.g., at 538°C).

The corrosion data indicate that dissolution of major alloy elements as well as chemical reactions (e.g., between nitrogen and chromium or iron) influence the corrosion behavior of ferrous alloys in flowing lithium. An increase in the nitrogen content in lithium from ~100 to 250 wppm increases the weight loss for both ferritic and austenitic steels. Corrosion products were detected on the alloy specimens. Data indicate that these products are ternary nitrides. The results also show some downstream effects on corrosion. Additional information on the influence of system parameters, such as lithium purity, system ΔT, location, etc., on the corrosion processes is needed to quantitatively establish the dissolution behavior of ferrous alloy in lithium.

Acknowledgment

The authors acknowledge the experimental contributions provided by R. H. Lee. The authors wish to thank V. A. Maroni for helpful discussions and the work in analytical chemistry. This work was supported by the Office of Fusion Energy, U. S. Department of Energy.

References

1. O. K. Chopra and D. L. Smith, J. Nucl. Mater. 133&134 (1985) 861.
2. P. F. Tortorelli, J. H. DeVan, and J. E. Selle, in: Proc. Second Intl. Conf. on Liquid Metal Technology in Energy Production, Richland, 1980, Ed. J. M. Kahlke, CONF-800401-P2 (U. S. Department of Energy, 1980) p. 13.44.
3. P. F. Tortorelli, J. H. DeVan, and J. E. Selle, in: Proc. Second Intl. Conf. on Liquid Metal Technology in Energy Production, Richland, 1980, Ed. J. M. Kahlke, CONF-800401-P2 (U. S. Department of Energy, 1980) p. 13.55.
4. P. F. Tortorelli and J. H. DeVan, J. Nucl. Mater. 103&104 (1981) 633.
5. P. F. Tortorelli and J. H. DeVan, J. Nucl. Mater. 122&123 (1984) 1258.
6. P. F. Tortorelli and J. H. DeVan, in: Proc. Third Intl. Conf. on Liquid Metal Technology in Energy Production, Oxford, 1984.
7. G. A. Whitlow, W. L. Wilson, W. E. Ray, and M. G. Down, J. Nucl. Mater. 85&86 (1979) 283.
8. D. G. Bauer, W. E. Stewart, I. N. Sviatoslavsky, and D. K. Sze, in: Proc. Second Intl. Conf. on Liquid Metal Technology in Energy Production, Richland, 1980, Ed. J. M. Kahlke (U. S. Department of Energy, 1980) p. 13.73.

9. F. Casteels, J. Dekeyser, M. Soenen, H. Tas, and J. Dresselaers, in: Proc. Third Intl. Conf. on Liquid Metal Engineering and Technology, Vol. 3, British Nuclear Energy Society, London (1985), p. 73.

10. H. U. Borgstedt, M. Grundmann, and J. Konys, Fusion Technology 8 (1985) 536.

11. O. K. Chopra, D. L. Smith, P. F. Tortorelli, J. H. DeVan, and D. K. Sze, Fusion Technology 8 (1985) 1956.

12. O. K. Chopra and P. F. Tortorelli, J. Nucl. Mater. 122&123 (1984) 1201.

13. P. F. Tortorelli and O. K. Chopra, J. Nucl. Mater. 103&104 (1981) 621.

14. O. K. Chopra and D. L. Smith, "Compatibility of Ferrous Alloys in Forced Circulation Pb-17Li System," these proceedings.

15. C. Tyzack and A. W. Thorley, in: Proc. Intl. Conf. on Ferritic Steels for Fast Reactor Steam Generators, British Nuclear Energy Society, London (1978) p. 241.

16. M. G. Barker, P. Hubberstey, A. T. Dadd, and S. A. Frankhaur, J. Nucl. Mater. 114 (1983) 143.

Table 1
Chemical compositions of austenitic and ferritic steels

Alloy	Content (wt %)									
	Cr	Ni	Mo	Mn	Si	P	S	C	N	Other
316 SS	17.0	13.4	2.49	1.9	0.64	0.024	0.020	0.07	0.034	
HT-9	12.0	0.6	1.03	0.5	0.22	0.006	0.002	0.21	0.003	0.32 V, 0.5 W
9Cr-1Mo	8.8	-	0.92	0.4	0.36	-	-	0.098	0.011	0.21 V, 0.06 Nb

Table 2
Lithium loop operating conditions for various corrosion tests

Test Run	Loop Temperature (°C)				N Content in Lithium (wppm)	Exposure Time (h)	
	Test Vessel	Spec. Exp. Vessel[a]	Supply Vessel	Cold Trap		Test Vessel	Spec. Exp. Vessel
1	482	482	432	212	<50	1295	5000
2	482/427[b]	482	407	230[c]	~250	-	1997
3	427	482	407	230	~100	1100	-
4	482	427	410	212	<100	5521	6501
5	427	372	372	206	~100	5023	4955
6	538	482	410	208	~50	3655	3330

[a]Lithium flow was from test vessel to specimen exposure vessel.
[b]Test vessel temperature changed from 482 to 427°C after 1540 h.
[c]No flow occurred through cold trap after 890 h due to plugging. Plugged sections were replaced and flow started after an additional 480 h.

Table 3
Weight loss and surface composition of HT-9 alloy exposed to flowing lithium

Test Run	Time (h)	Temp. (°C)	Weight Loss (g/m^2)	Surface Composition (%) Cr	Fe
-	Unexposed		-	12.0	85.6
6	2271	538	2.13	5.8	93.3
1	1295	482	0.30	10.8	86.8
1	3000		1.35	6.2	91.8
1	5000		0.82	6.6	91.3
2	1997		2.93	7.1	88.5
4	5521		1.83	5.9	88.4
6	1707		0.28	8.6	89.1
6	2528		0.0	8.8	88.2
3	1100	427	0.22	11.0	87.0
4	5739		1.17	8.1	87.1
4	5739		1.11	8.7	84.8
4	6501		0.85	7.3	90.7
5	5023		1.37	6.5	88.4
5	4955	372	0.58	8.3	89.7
5	4955	372	0.65	8.0	87.8

Table 4
Weight loss, depth of internal penetration, and surface compositions of annealed Type 316 SS exposed to flowing lithium

Test Run	Time (h)	Temp. (°C)	Weight Loss (g/m^2)	Ferrite Layer (μm)	Surface Composition (%) Cr	Fe	Ni
-	Unexposed	-	-	17.5	64.9	12.9	
6	2271	538	5.9	-	9.7	83.9	2.5
6	2271		13.3	-	8.7	88.4	0.4
6	3185		8.9	-	9.9	85.2	2.2
1	1295	482	6.7	13.0	12.2	81.6	1.2
2	1997		21.0	25.0	6.2	90.9	1.1
4	5521		31.8	37.0	9.7	84.0	0.7
6	619[b]		4.8	-	22.0	68.7	2.3
6	619[a]		4.8	-	15.4	73.4	6.0
6	1707[b]		12.7	-	20.2	74.6	0.7
6	3330[b]		19.8	-	20.1	73.0	0.8
3	1100[a]	427	17.2	21.0	18.7	77.1	1.8
4a	5739		42.2	38.0	8.3	88.4	0.9
4b	5739		41.5	37.0	8.1	86.6	0.8
5	5023		57.2	31.0	8.0	90.6	0.6
5a	4955	372	14.1	9.0	10.6	86.0	1.4
5b	4955	372	12.9	13.0	9.7	87.3	1.5

[a]Large deposits of chromium observed on the specimen. The surface composition represents regions away from the deposits.
[b]Average composition of the surface with deposits.

Table 5
Dissolution rates of ferritic and austenitic steels exposed to flowing lithium

Test Run	Specimen Location[a]	Temp. (°C)	Maximum Time (h)	Dissolution Rate ($mg/m^2 \cdot h$) HT-9	9Cr-1Mo	316 SS	316 CW
4	Test Vessel	482	5521	0.173	0.144	1.61	1.58
4	Spec. Exp. Vessel	427	5739	0.064	0.066	2.21	2.18
	Spec. Exp. Vessel	427	6501	0.070	0.070	-	-
5	Test Vessel[b]	427	5023	0.077	0.062	9.17	6.34
5	Spec. Exp. Vessel	372	4955	0.029	0.030	2.11	2.48
6	Test Vessel	538	3655	0.401	0.391	2.05	1.41
	Test Vessel	538	2271	-	-	1.75	-
6	Spec. Exp. Vessel[c]	482	3330	-	-	2.05	1.84

[a]Corrosion specimens were exposed in the test and specimen exposure vessels. Lithium flow was from test vessel to specimen exposure vessel.
[b]Dissolution rates for HT-9 and 9Cr-1Mo were obtained from combined data of Runs 4 and 5.
[c]Large deposits were observed on specimen surfaces. Ferritic steels showed little or no weight loss.

Table 6
Spectrochemical analysis of methanol used for cleaning corrosion specimens exposed to lithium at 538 and 482°C

Alloy	Major Elements (wppm)							
	538°C				482°C			
	Cr	Fe	Ni	Mo	Cr	Fe	Ni	Mo
HT-9	19	67	<15	10	42	33	<15	12
316 SS	46	68	13	135	207	31	14	60
Lithium	<5	17	13	<10	<5	18	<15	<10

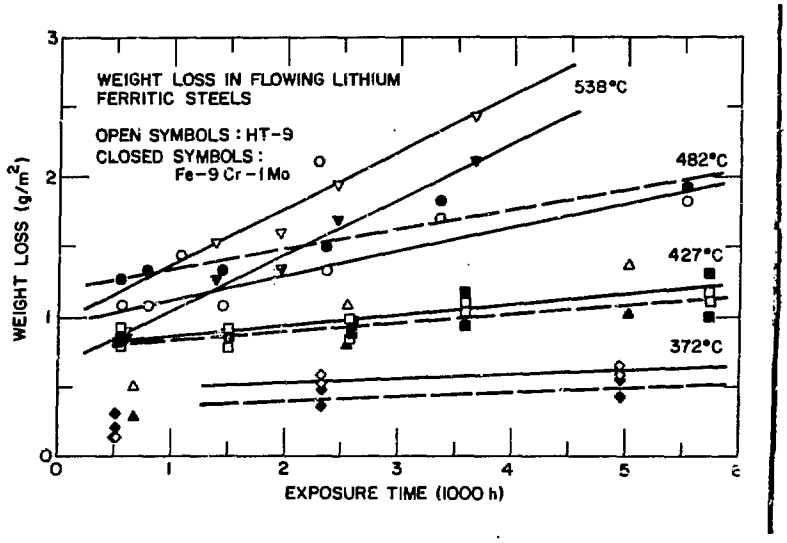

Fig. 1. Weight loss versus exposure time for HT-9 and Fe-9Cr-1Mo ferritic steels exposed to flowing lithium.

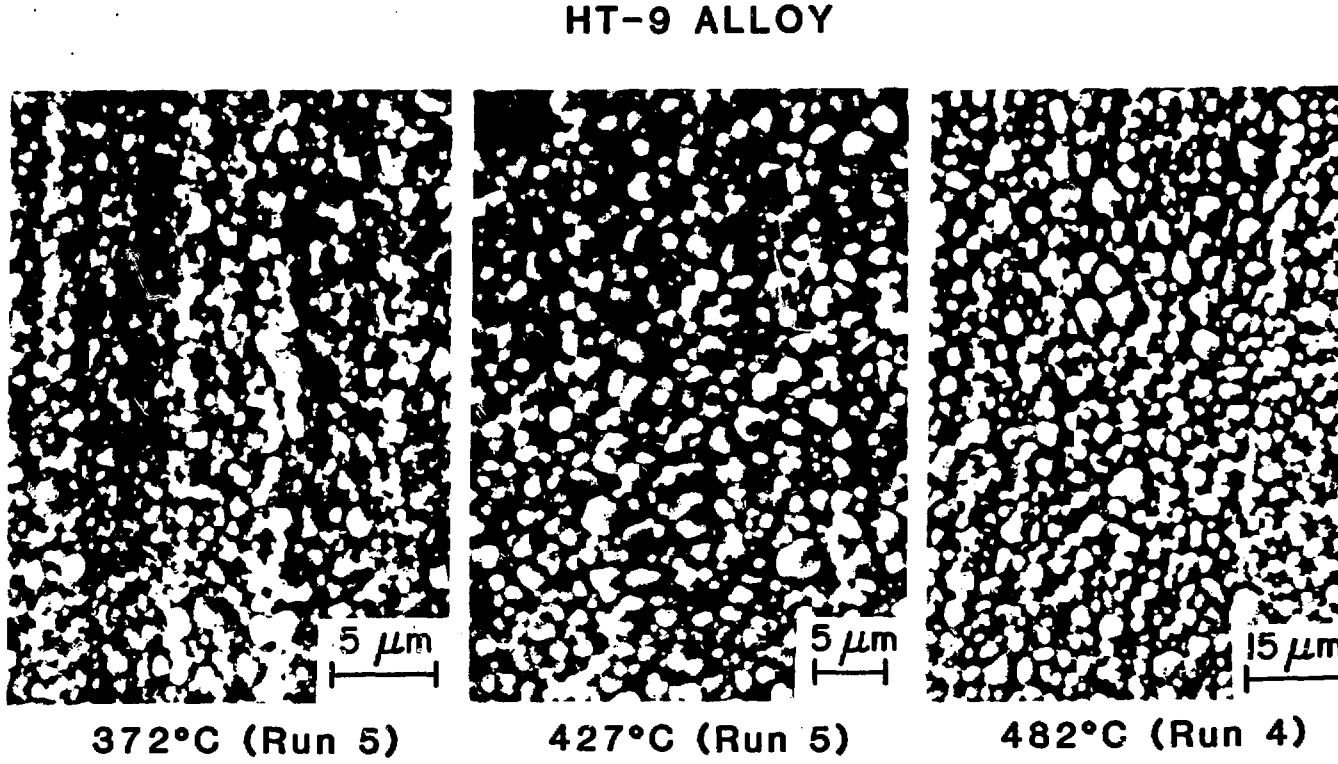

Fig. 2. Micrographs of HT-9 alloy surface exposed to flowing lithium for ~5000 h at 372, 427, and 482°C.

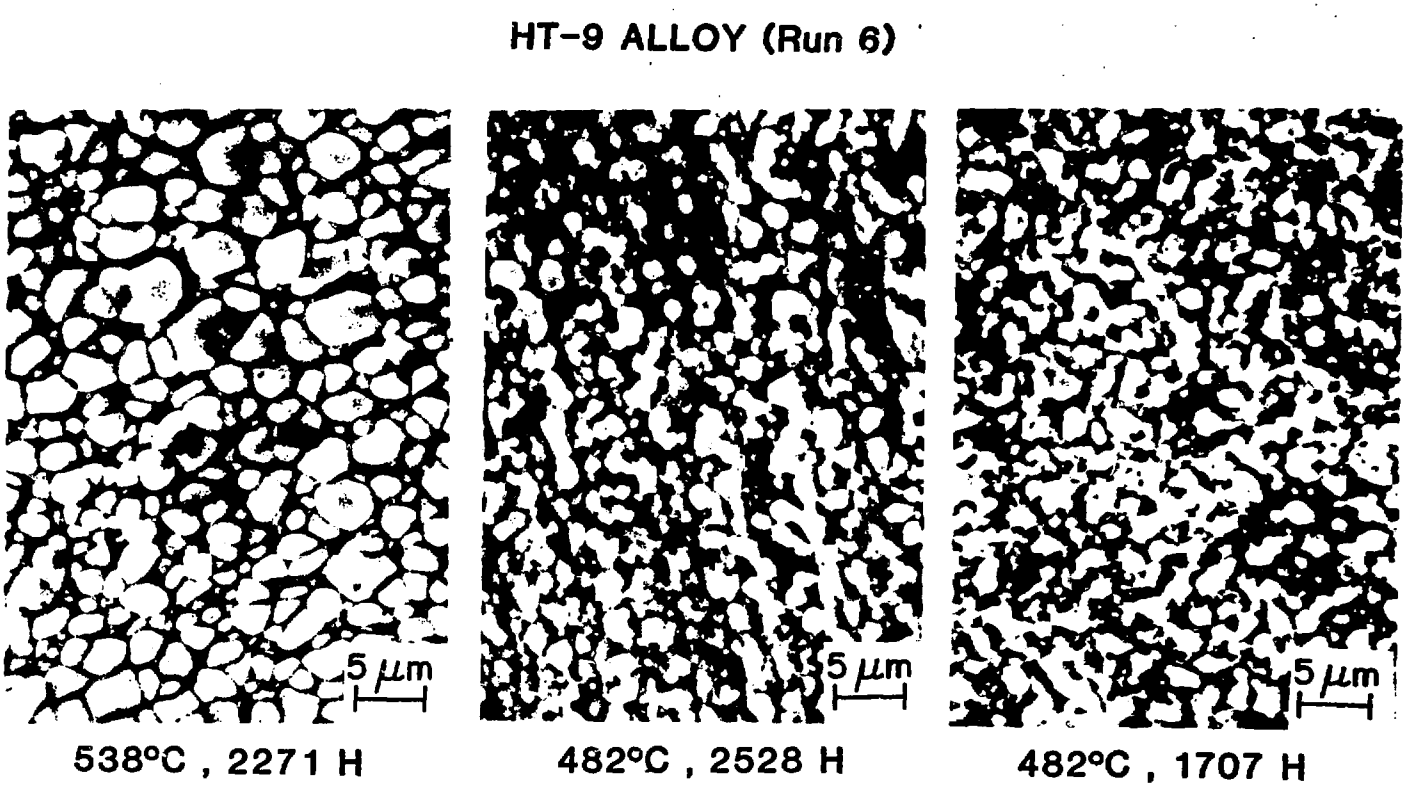

Fig. 3. Micrographs of HT-9 alloy surface exposed to flowing lithium at 538 and 482°C, run 6.

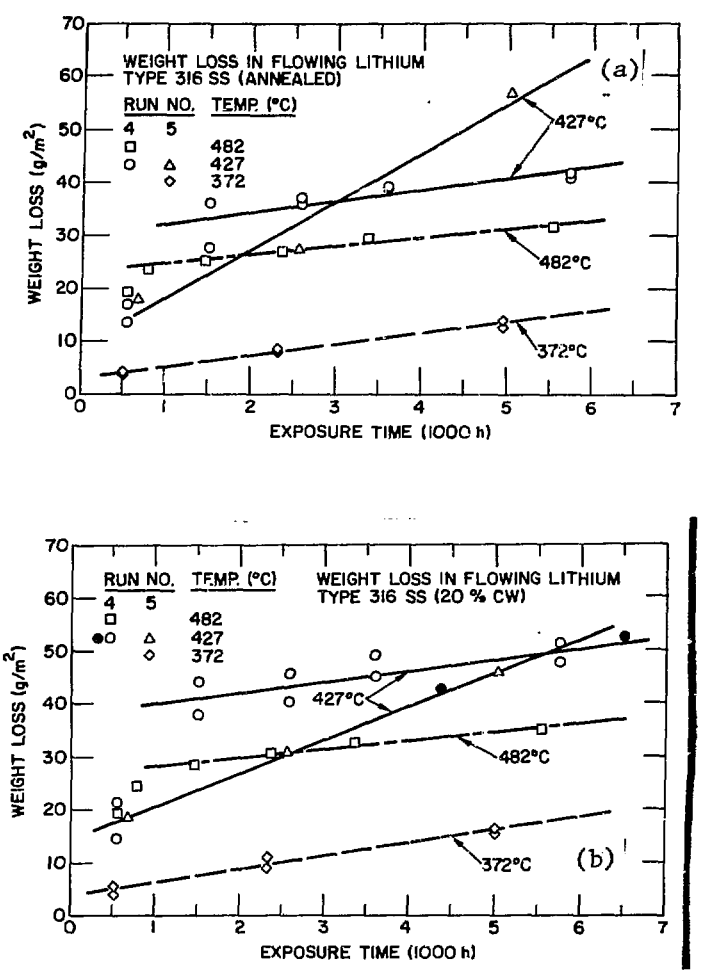

Fig. 4. Weight loss versus exposure time for (a) annealed and (b) 20% CW Type 316 stainless steel exposed to flowing lithium at 372, 427, and 482°C.

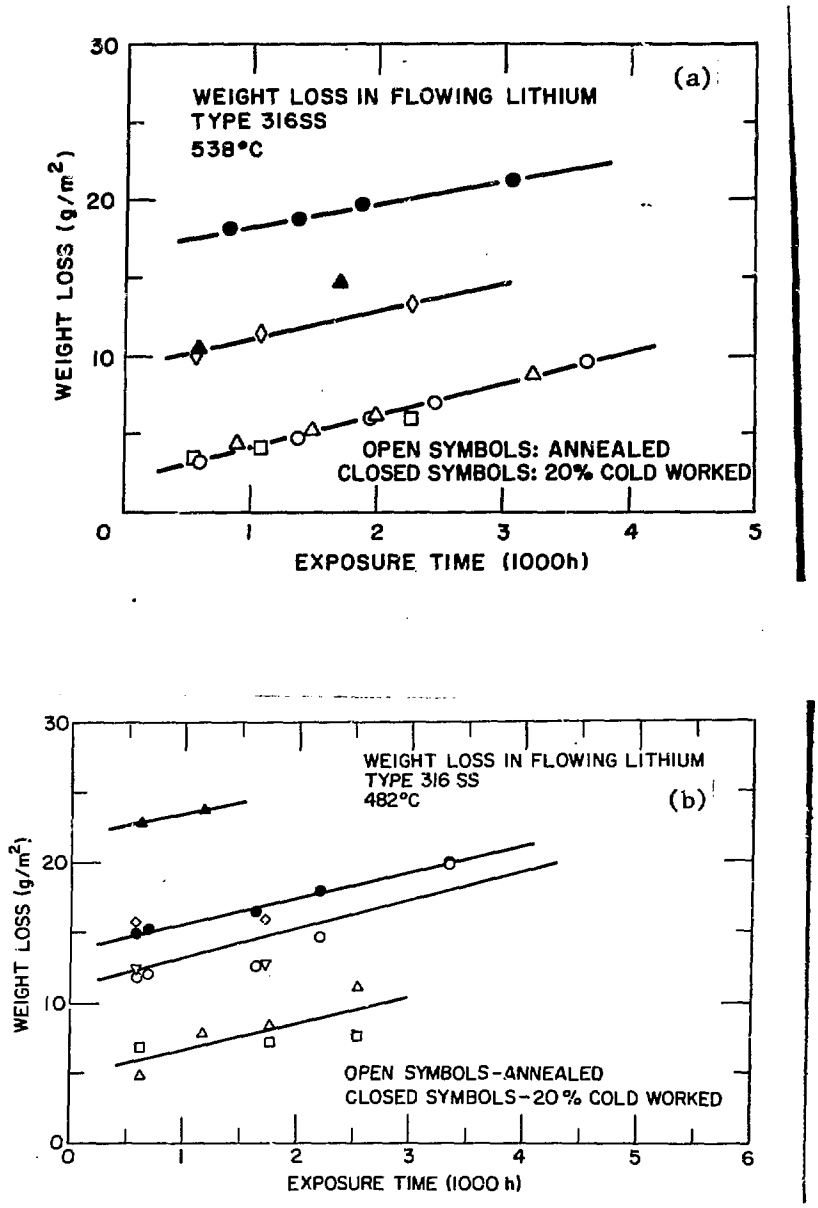

Fig. 5. Weight loss versus exposure time for annealed and 20% CW Type 316 stainless steel exposed to flowing lithium during run 6. (a) In the test vessel at 538°C and (b) downstream in the specimen-exposure vessel at 482°C.

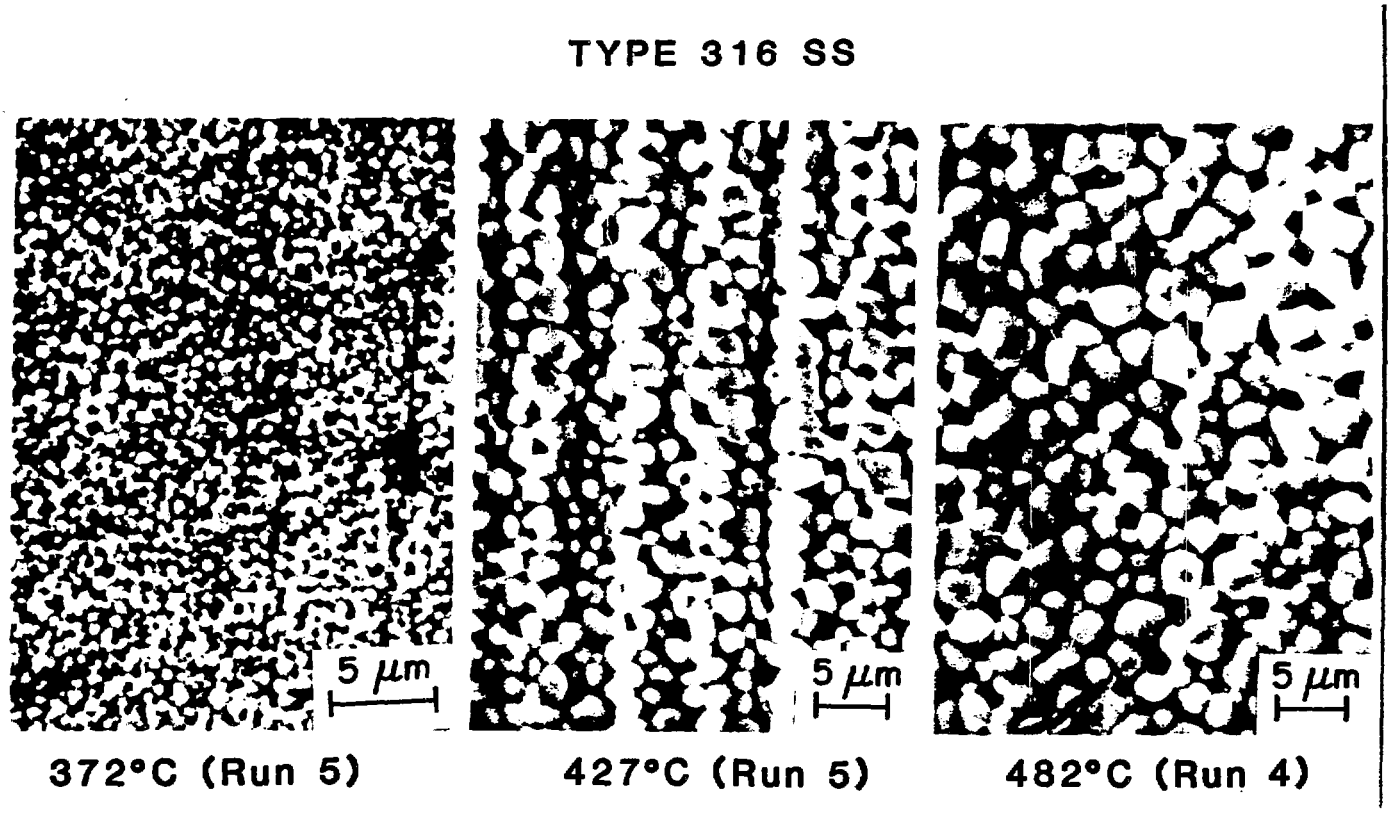

Fig. 6. Micrographs of the surface of annealed Type 316 stainless steel exposed to flowing lithium for ~5000 h at 372, 427, and 482°C.

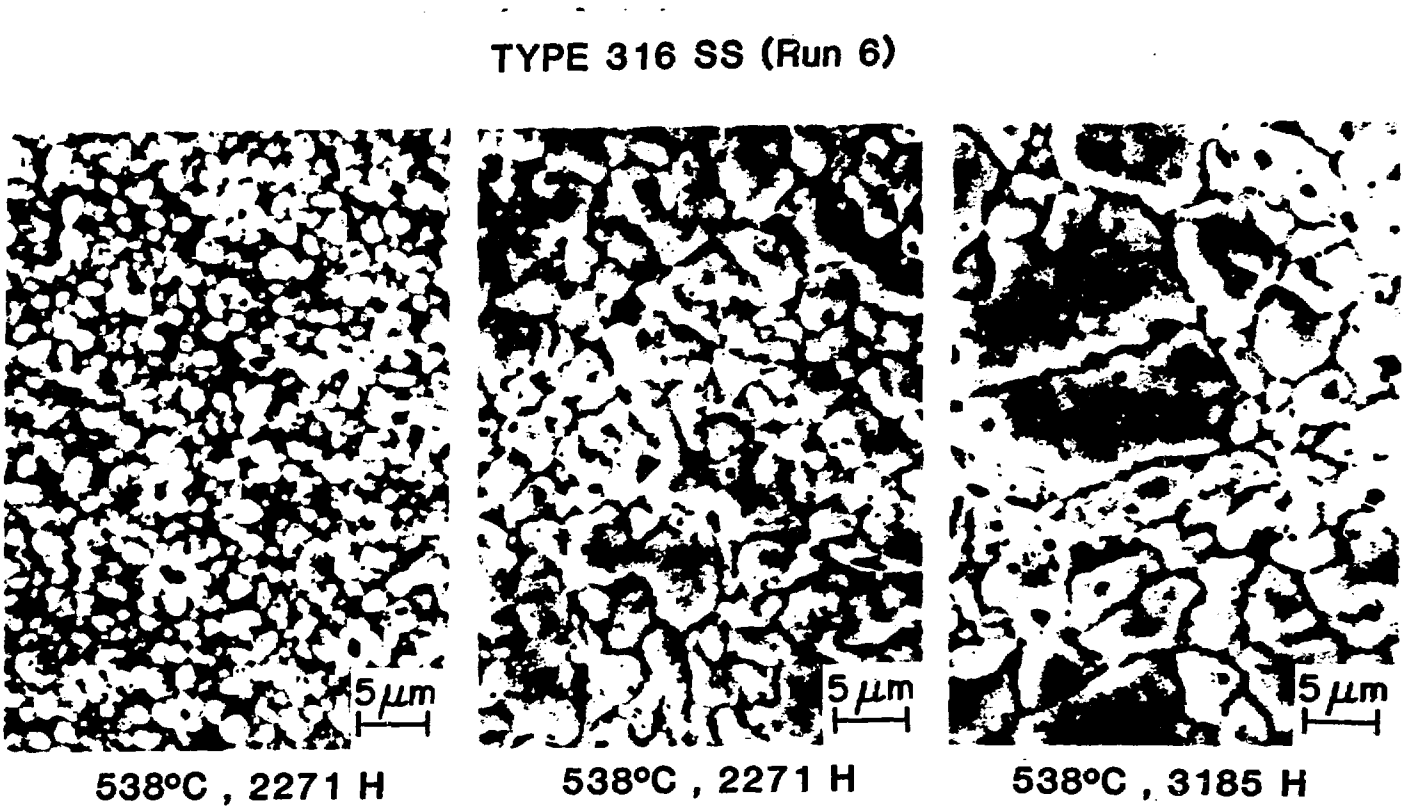

Fig. 7. Micrographs of the surface of annealed Type 316 stainless steel exposed to flowing lithium at 538°C, run 6.

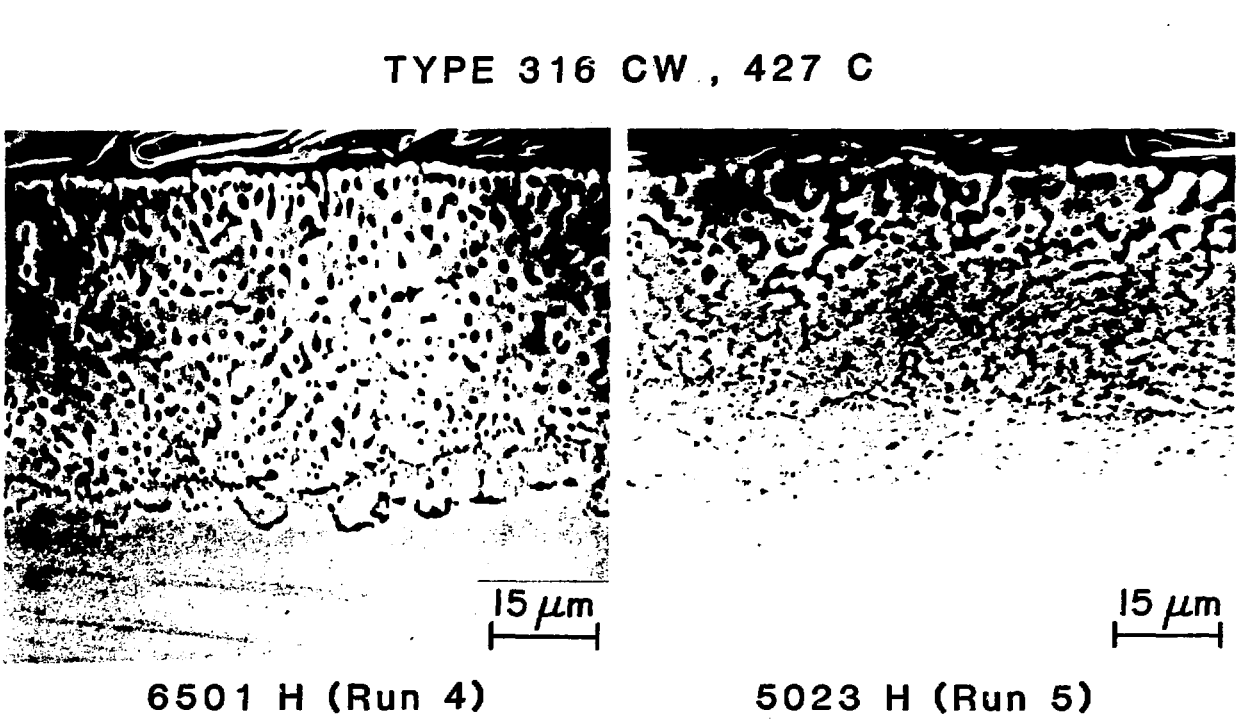

Fig. 8. Micrographs of the ferrite layers formed on 20% CW Type 316 stainless steel exposed to lithium for >5000 h at 427°C during runs 4 and 5.

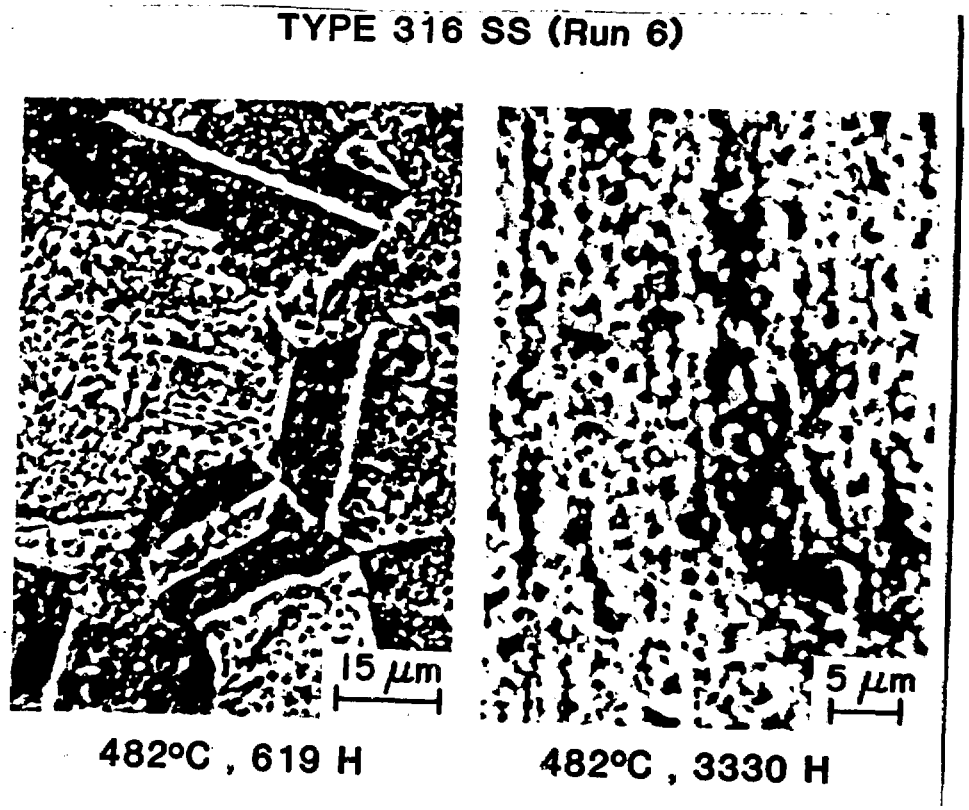

Fig. 9. Micrographs of the surface of annealed Type 316 stainless steel exposed in the specimen exposure vessel at 482°C, run 6.

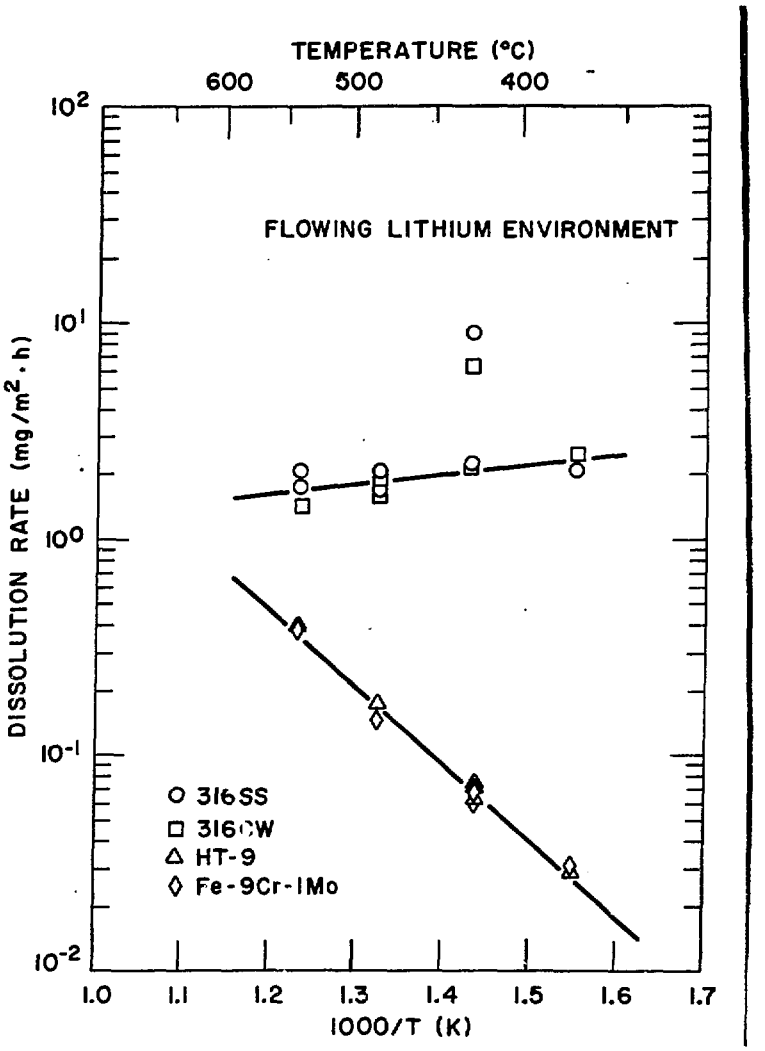

Fig. 10. Arrhenius plot of dissolution rate data for ferritic and austenitic steels exposed to flowing lithium.